Journal of Materials Chemistry B

PAPER

Screening of bio-compatible metal–organic frameworks as potential drug carriers using Monte Carlo simulations†

Cite this: J. Mater. Chem. B, 2014, 2, 766

María C. Bernini,[ab] David Fairen-Jimenez,*[bc] Marcelo Pasinetti,[a] Antonio J. Ramirez-Pastor[a] and Randall Q. Snurr[b]

Received 25th September 2013
Accepted 22nd November 2013

DOI: 10.1039/c3tb21328e

www.rsc.org/MaterialsB

A series of bio-compatible metal–organic frameworks (MOFs) have been studied as potential carriers for drug delivery applications. Grand canonical Monte Carlo (GCMC) simulations were performed to study the adsorption of the model drug ibuprofen. Simulations were first validated with available experimental data for ibuprofen adsorption and release in MIL-53, MIL-100 and MIL-101. In the second stage, the study was extended to three additional MOFs with interesting properties in terms of bio-compatibility and porosity: CDMOF-1, based on edible precursors; MOF-74 containing a highly biocompatible metal (Mg); and BioMOF-100, a mesoporous MOF with extremely high pore volume. By comparing with experimental data, we show how GCMC simulation is able to predict the macroscopic performance of new porous MOFs in drug delivery applications, providing useful molecular-level insights and giving thermodynamic and structural details of the process. Adsorption isotherms, snapshots, energy of adsorption and radial distribution functions were used to analyse the drug delivery process.

Introduction

The study of the molecular mechanisms that control drug delivery in porous systems is of critical importance to nanomedicine applications, where nanotechnology has the potential to revolutionise cancer diagnosis and therapy.[1] Indeed, a fundamental, yet unresolved problem in many therapies including cancer treatment is that many routinely used therapeutic agents present a high-level concentration within the first minutes after dosing, followed by low-levels in the next hours. Nanomedicine systems aim to improve the biodistribution of therapeutic agents, so the efficacy of the intervention can be increased while their toxicity is attenuated. To develop therapeutic agents that can achieve this aim, a large number of drug delivery systems such as polymer–protein conjugates, immunotoxins (fusion proteins), chemo- and radio-immunoconjugates, liposomes, dendrimers and micelles have been suggested in recent years.[2] However, most of the proposed routes suffer from important drawbacks such as low drug capacity or poor control of release kinetics.

Recently, metal–organic frameworks (MOFs) have been proposed as nano-carrier platforms for drug-delivery.[3] MOFs are obtained by the self-assembly of metal clusters and organic linkers, resulting in tailored nanoporous host materials with pore sizes up to 6 nm. MOFs with extraordinary pore volumes show great promise in nanomedicine applications due to their interesting porous and structural properties.[4,5] One of the most striking advantages of MOFs over more traditional porous materials is the possibility of tuning the host–guest interaction, not only by varying their pore size but also by functionalizing the building blocks with chemical groups, providing the possibility of controlling the kinetic release of a therapeutic agent. MOFs offer extremely high drug capacity (*e.g.* up to 1.4 g of ibuprofen per gram of porous solid: four times higher than the adsorption achieved with mesoporous silica materials) and very long release times (*e.g.* up to 21 days) of several therapeutic agents.[3a–d] In particular, Horcajada *et al.* found a remarkably good activity when using MOF nanoparticles charged with busulfan for the treatment of human leukemia and multiple myeloma, or charged with AZT-TP as an anti-HIV agent.[3d] Morris *et al.* have shown the possibility of using MOFs for the adsorption and controlled release of gas transmitter agents such as NO for antithrombosis and vasodilatation.[6] Lin *et al.* used Mn-based MOFs as contrast agents for magnetic resonance imaging and also an amino-functionalised version of MIL-101(Fe) as a carrier of a pro-drug based on cisplatin,

[a]Departamento de Física, Instituto de Física Aplicada, Universidad Nacional de San Luis CONICET, San Luis, Argentina

[b]Department of Chemical and Biological Engineering, Northwestern University, Evanston, Illinois, USA

[c]Department of Chemical Engineering and Biotechnology, University of Cambridge, Pembroke St., Cambridge CB2 3RA, UK. E-mail: df334@cam.ac.uk; Web: http://people.ds.cam.ac.uk/df334

† Electronic supplementary information (ESI) available: MOF biocompatibility (median lethal dose, LD50), description of the MOF structures, nodes and linkers, force field parameters, radial distribution function (RDF) plots, adsorption snapshots and videos showing the adsorption mechanism in MIL-101 and BioMOF-100. See DOI: 10.1039/c3tb21328e

showing a comparable cytotoxicity to that of the isolated administrated cisplatin drug.[7]

Given the many different MOF structures, a systematic study of their performance in drug delivery is essential for the identification of promising structures. Molecular simulations provide an outstanding tool to predict the performance of the materials and, thus, to select the optimal structures for a given application. Grand canonical Monte Carlo (GCMC) simulation is the workhorse for simulating adsorption in porous materials, explaining and predicting new experimental results. However, the simulation of large guest molecules, *e.g.* a drug, is difficult because of the tight fit of the molecules in the pores. As a consequence, the reported modeling studies on drug-porous solid systems are rather scarce.[8] For example, Fatouros *et al.* studied the diffusion properties of salbutamol and theophylline in the zeolite BEA using molecular dynamics (MD), showing that MD modeling can be used for screening purposes in zeolite–drug combinations prior to experimental investigation.[9] Looking at the MOF family, only a small number of computational studies have been carried out. These studies focused on one or two structures simultaneously, limiting the possibilities of correlating drug delivery performance with different structural features such as pore volume, pore size distribution (PSD) and shape, *etc.* Horcajada *et al.* used Density Functional Theory (DFT) calculations to identify the most favorable conformations and adsorption sites of ibuprofen[3b] and busulfan[10] on MIL-53(Fe). Gaudin *et al.* used quantitative structure–activity relationship (QSAR) models to rationalise the experimental uptake of the model drug caffeine in a series of flexible iron terephthalate MIL-88B(Fe) materials with different functional groups.[11] Babarao and Jiang used computational methods to study the energetics and dynamics of ibuprofen in MIL-101 and UMCM-1.[12] They also performed simulated annealing followed by DFT of one single ibuprofen molecule to study the preferential adsorption sites. However, to the best of our knowledge, no experimental or computational studies have been carried out to study the adsorption mechanisms of drugs on MOFs and to analyse the influence of the MOF textural properties such as pore volume and PSD in the drug adsorption–delivery phenomena on MOFs.

In this work, we used GCMC simulations to screen a series of bio-compatible MOFs as carrier systems of a model drug, the anti-inflammatory and analgesic ibuprofen (α-*p*-isobutylphenylpropionic acid), IBU. We validated our results with the available experimental data reported for the adsorption–release of ibuprofen in MIL-53(Fe),[3b] MIL-100(Fe),[3a,d] and MIL-101(Cr).[3a,d] Note that even though chromium is a very toxic metal, we used these experimental data for proof-of-concept validation. Indeed, the homologous nontoxic iron MIL-101 exists in the literature.[13] We extended our study to three novel bio-compatible MOFs based on non-toxic metals, MOF-74(Mg),[14] edible carbohydrate linkers, CD-MOF1,[15] and outstanding pore volumes, BioMOF-100.[5] The MOFs were also chosen to represent a wide range of textural properties: MIL-53, MOF-74 and CDMOF-1 are microporous materials; MIL-100 and MIL-101 are mesoporous materials with narrow microporous windows; and BioMOF-100 is a strictly mesoporous MOF. We focused on the maximum adsorption capacity of each MOF; the shape of the simulated adsorption isotherms (*e.g.* the existence or not of steps during the adsorption process); the siting of the drug molecules in the porous structures through the analysis of snapshots and radial distribution functions (RDF); and the loading-release dependency on the average potential energy of adsorption (U_{gh}) of IBU inside the MOFs. We explored these materials as potential drug vehicles by comparing their performance with state-of-the-art MOFs for such applications.

Results and discussion

2.1. Ibuprofen capacity screening

Table 1 summarises the textural properties of the proposed MOFs: surface area, void fraction, pore volume and calculated pore size distribution (PSD). Fig. S1–S4 in the ESI† show their structures. The BET surface areas and pore volumes range from 877 (MOF-74) to 4500 (MIL-101) $m^2\ g^{-1}$ and from 0.48 (MIL-53) to 2.90 $cm^3\ g^{-1}$ (BioMOF-100), respectively.

Fig. 1 (top) shows the broad range of PSDs in the selected MOFs, where MIL-53, CDMOF-1 and MOF-74 are microporous and MIL-100, MIL-101 and BioMOF-100 are mesoporous. It is worth mentioning that MIL-100 and MIL-101 present microporous windows between the main cavities.

Fig. 1 (bottom) and S5† present the adsorption isotherms of IBU on the selected MOFs. The sequence of the isotherms is related to the PSD and the surface chemistry of the MOFs, where CDMOF-1 and MIL-53, on one hand, and BioMOF-100 and MIL-101, on the other hand, start adsorbing at the lowest and highest pressure, respectively. In general, these materials with smaller pores present higher loadings at lower pressure due to the higher adsorbate–adsorbent (*i.e.* IBU–MOF) interactions provoked by the overlap of the adsorption potential of the pore walls. However, the presence of strong electrostatic interactions due to the existence of charge-compensating ions in CDMOF-1 (OH^- groups) and BioMOF-100 (dimethylammonium, DMA, cations) enhances the adsorbate–adsorbent interactions and induces the adsorption of IBU at lower fugacities than other MOFs with smaller pores (see for example CDMOF-1 *vs.* MIL-53).

To validate our simulations, we first compared the trends obtained between the pore volume and maximum loading. Fig. 2 shows an excellent agreement. Remarkably, BioMOF-100 presents an outstanding IBU capacity of 1975 mg g^{-1}, which is six and thirteen times higher than the values found for mesoporous silicas[18] and zeolites (*e.g.* dealuminated faujasites),[19] respectively. When comparing with the experimental data, the simulated capacities for MIL-53 and MIL-101 perfectly match the experimental values with differences below 6%. In contrast, the experimental maximum loading of MIL-100 falls under the general trend, being almost half (*i.e.* 48%) of the simulated value. MIL-53 shows regular channels of *ca.* 7.4 Å diameter, whereas MIL-101 shows spherical mesoporous cages accessible through pentagonal and hexagonal windows of *ca.* 12 and 16 Å. In both cases, the accessibility of IBU molecules (*ca.* 5 × 10 Å size) to the material's porosity should be easily achievable. In contrast, the spherical mesoporous cages of MIL-100 are connected by narrower cavities: the larger ones by *ca.* 8.5 Å

Table 1 Textural properties, pore size distributions (PSD), simulated and experimental maximum ibuprofen uptakes of the MOFs under study

	Calculated pore volume ($cm^3\ g^{-1}$)	Pore-cavity size (Å)	Experimental surface area (BET, $m^2\ g^{-1}$)	Maximum simulated uptake (molecules per cell)	Maximum simulated uptake (mg g^{-1})	Maximum experimental uptake (mg g^{-1})
MIL-53	0.479	7.4[3b]	(—)[a]	1	231	220[3b]
CD-MOF-1	0.493	7.8; 17[15]	1220[15]	23	274	—
MOF-74	0.793	12[14]	877[14]	4.8	425	—
MIL-100	1.030	25; 29[17]	2100[17]	125	645/403	330[3a,d]
MIL-101	2.218	29; 34[16]	4500[17]	280	1291	1376[3a,d]
BioMOF-100	2.905	28[5]	4300[5]	581	1975	—

[a] This material does not show any porosity for N_2 at 77 K.[3b]

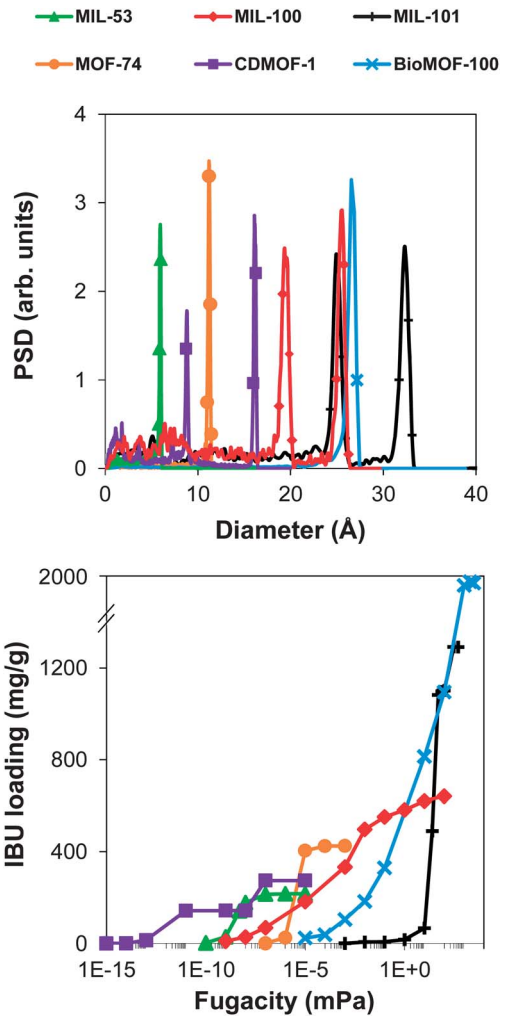

Fig. 1 (top) Pore size distribution (PSD) calculated from the crystal structures using the method of Gelb and Gubbins[16] (bottom) and simulated ibuprofen adsorption isotherms at 310 K in a series of MOFs.

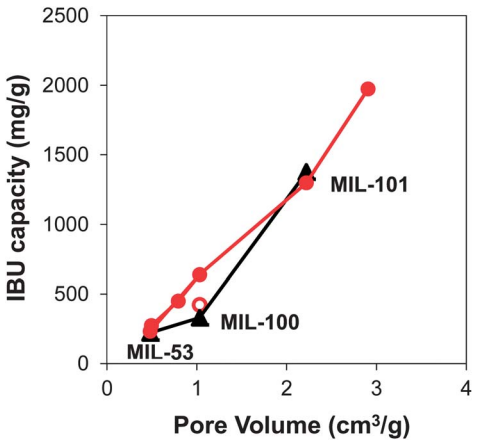

Fig. 2 Simulated (red circles) and, when available, experimental (black triangles) ibuprofen capacities for the selected series of MOFs *vs.* their calculated pore volumes. The red open circle represents the simulation on MIL-100 with blocked cavities.

hexagonal windows and the smaller ones by *ca.* 5 Å. In this case, the accessibility to the smaller mesoporous cages might be kinetically impeded by the narrow size due to the dynamic uptake process. In this line, the observed experimental low capacity of MIL-100 was explained in the original study by the existence of diffusional problems through the narrow pentagonal windows during the experiment, impeding the access of IBU to the smaller mesoporous cavities of MIL-100.[3a,17] This phenomenon is in principle not captured by GCMC simulations, where the entire void volume, accessible or not, is taken into account during the simulation. In order to confirm the existence of dynamic issues during the filling process that could justify the difference in the simulated and experimental uptake values, we ran a new simulation on MIL-100 blocking the adsorption of IBU in the smaller mesoporous cavities. Fig. S6† in the ESI shows the comparison between both simulations. The most appreciable difference in the new isotherm is a significant decrease in the maximum loading down to 403 mg g^{-1}, still higher, though, than the experimental value (*i.e.* experimental capacity, 330 mg g^{-1}, is still 18% lower). Deviations from computationally observed trends after blocking the smaller mesoporous cavities of MIL-100 suggest that the non-accessibility of these cavities to IBU exists, but is not enough to explain the experimental results, and the difference might reflect experimental issues during the drug loading or difficulties in sample activation.[20] This fact indicates that the potential of MIL-100 as a drug carrier could be slightly higher than what was previously obtained experimentally.

2.2. Ibuprofen adsorption mechanism

The profile of the simulated isotherms shown in Fig. 1 can be understood in terms of different adsorption regimes. First, for microporous MIL-53 and MOF-74 there is very little uptake at

low pressure, followed by a sharp jump in the loading corresponding with the saturation in the 1D uniform channels, as shown in Fig. 3 and S17.† This phenomenon is characteristic of systems where the adsorbate–adsorbent interactions are strong relative to the adsorbate–adsorbate interactions.[21a]

The analysis of the RDF obtained for ibuprofen on MIL-53 (see Fig. S7, S9 and S10, ESI†) shows that the most relevant interaction involves a weak H-bond with the carboxylic group of MIL-53 (*i.e.* O_a indicated in Fig. S7†), along with a strong interaction with the Fe(III) when the loading achieves saturation. In the case of MOF-74, the RDF analysis (see Fig. S11†) shows that the most important interactions can be divided into two types: on one hand, those involving the oxygen atoms of MOF-74 (O_b and O_c, see Fig. S7†) as H-bond acceptors and, on the other hand, those concerning the coordinatively unsaturated Mg sites. The resultant distances are comparable with those found for H-bonds in crystals[22] and slightly higher than Mg–O coordination bonds, respectively. In both MIL-53 and MOF-74 cases, there is a cooperative interaction between the pore walls that involves a synergic adsorption effect, giving rise to a strong drug confinement in the small one-dimensional pores. It is known that the overlapping of the adsorption potentials in narrow micropores results in adsorption energies that can be double the corresponding values for an open surface.[21]

In the case of CDMOF-1, the adsorption isotherm exhibits two well-defined steps. Snapshots of the adsorption process presented in Fig. 4 and S18† reveal the adsorption of the first molecules in the narrow cylindrical channels of *ca.* 7.8 Å in diameter, followed by the saturation of the main cavities of *ca.* 17 Å in diameter. As in the previous MIL-53 case, RDF analysis represented in Fig. S12† indicates that the most important interactions involve the metal centers and the carbonyl oxygen atom of IBU molecules. Fig. 5 and S19† show the snapshots obtained at different loadings on MIL-101 and MIL-100, respectively. Videos of the adsorption process at different uptakes are included in the ESI.† The adsorption of the first IBU molecules takes place on the surface of both small and large mesoporous cages present in MIL-100 and MIL-101. In the case of MIL-100, the very initial molecules are adsorbed in the proximity of the narrow windows of *ca.* 5 Å size where the coordinatively unsaturated Fe sites are pointing (Fig. S20†), acting as primary adsorption sites along with the coordinated fluorine atoms, leading to a reinforcement of the interactions in these areas. Even if we used a non-parameterised force field as a first approximation for screening purposes, our simulation approach was able to reproduce the high interactions existing with the metal. As can be seen from the snapshots, this situation does not arise in the case of MIL-101, mainly due to the larger window size (*ca.* 12 Å) and to the fact that the unsaturated metal sites are not pointing to the windows but to the centre of the cavities (Fig. S21 and S22†). When the IBU loading

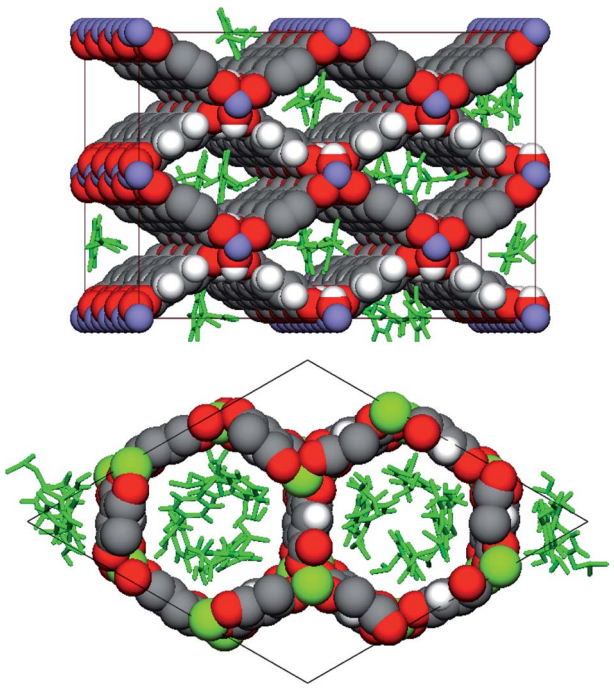

Fig. 3 Snapshots of ibuprofen in MIL-53 (top) and MOF-74(Mg) (bottom) at saturation. Ibuprofen molecules are shown in green stick-mode.

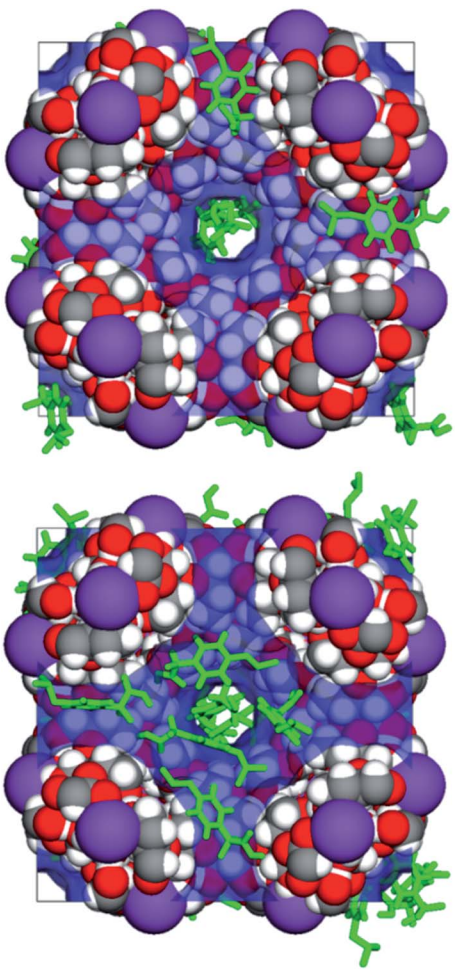

Fig. 4 Snapshots of adsorbed ibuprofen molecules in CDMOF-1 at different loadings: 143 mg g^{-1} (top) and 274 mg g^{-1} (bottom). Ibuprofen molecules are shown in green stick-mode. The accessible surface is shown in blue.

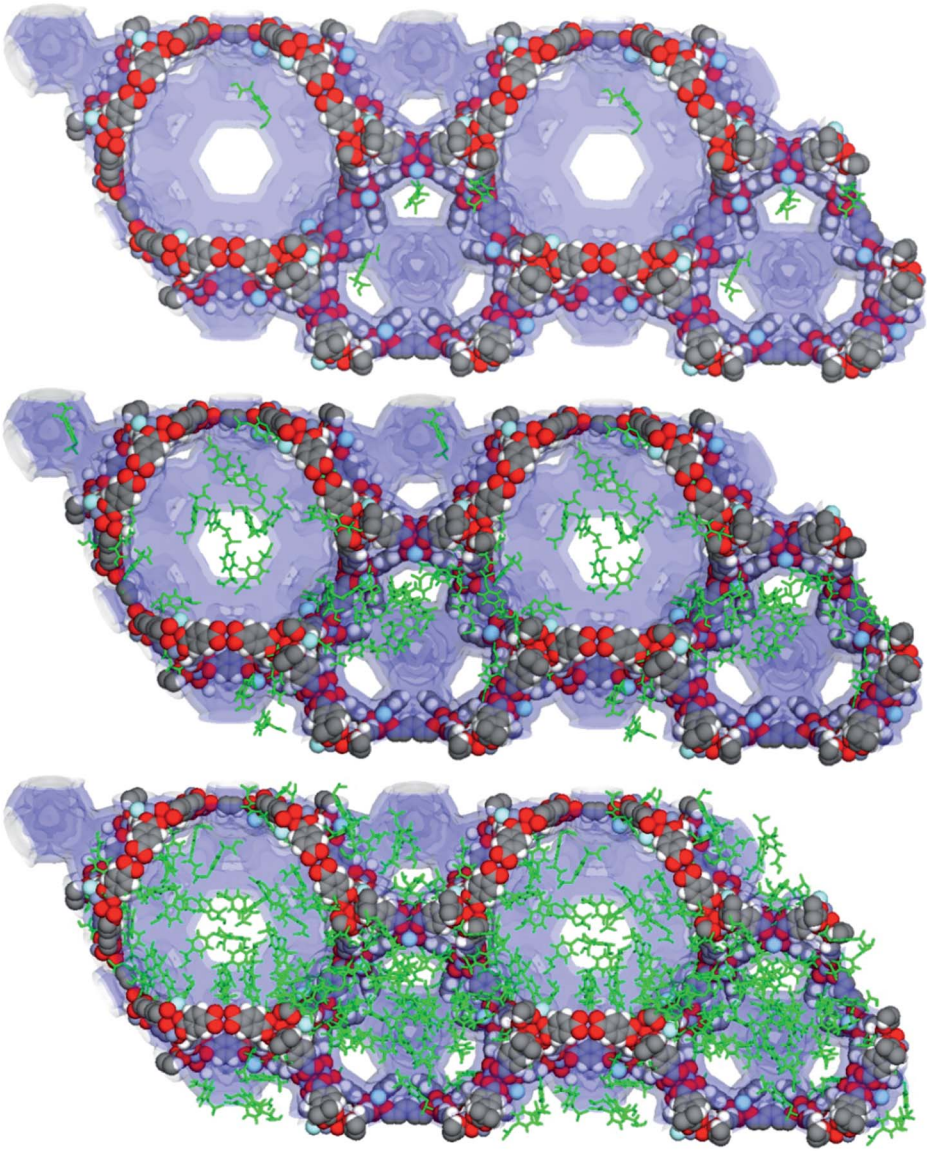

Fig. 5 Snapshots of ibuprofen in MIL-101 at different uptakes: 66 mg g^{-1} (top), 490 mg g^{-1} (center) and 1102 mg g^{-1} (bottom). Only a slice of the structure has been represented for clarity. Ibuprofen molecules are shown in green stick-mode. The accessible surface is shown in blue.

increases, the spherical cavities are gradually filled, increasing the drug–drug interactions and leading to the saturation of the pores. This fact is discussed further in the next section in the analysis of the average potential energy of IBU inside the host frameworks U_{gh}. In the case of the simulation of MIL-100 with IBU molecules start adsorbing on the surface of the accessible, larger cavities before the condensation process in the pores.

Regarding the RDF analysis, both MIL-100 and MIL-101 present similar anchoring points due to the high similarity between their structures. Fig. S13a and S14a† reveal that the distance between the IBU's carboxylic group and the metal cluster decreases when increasing the loading. Since the coordinatively unsaturated metals are pointing to the centre of the windows and the main cavities in MIL-100 and MIL-101, respectively, the adsorption mechanism is however affected.

The final distance of *ca.* 2 Å for pairs O_a–H between the MOF and the IBU (see Fig. S7, S13-a and S14-a†) is typical of H-bonds of moderate strength, corresponding to predominantly electrostatic interactions.[22] In addition, Fig. S13-b and S14-b† show a steady short distance between the IBU's hydrogen atom of the carboxylic group and the coordinated fluorine atoms localised in the narrow windows during the whole loading range. This confirms the previous observation about the preferred primary adsorption sites at very low loadings. Regarding the IBU–IBU interaction, the distance between carboxylic groups of different IBU molecules (O–H···O=C, see Fig. S9†), represented in Fig. S15,† decreases dramatically when the loading increases, showing a high tendency to form strong H-bonds and to condense at high loadings. The BioMOF-100 simulations reveal a typical adsorption process of a mesoporous material. Fig. 6 shows a gradual filling: at very low loadings, a monolayer of IBU

is gradually formed on the surface, followed by a multilayer filling process until *ca.* 50% of the total uptake. After that, a condensation of the IBU molecules in the center of the pores takes place. Videos are included in the ESI.† During this process, the RDF in Fig. S16† reveals that IBU molecules interact as the H-donor with the MOF oxygen atoms at all loadings, but also the DMA cations present strong interactions with the framework's oxygen atoms and the IBU's carboxylic group. In this way, the interactions of IBU molecules are increased due to the existence of cation–anion pairs in the MOF. This is in agreement with the position of the isotherm, since it starts to grow at much lower fugacity values than what is expected by comparing its pore size with *e.g.* MIL-101. The tendency to increase the magnitude of the H-bond interaction between different carboxylic groups of IBU molecules (O–H···O=C) is evident even at very low loadings. This can be associated with the marked increase of the adsorbate–adsorbate component of the U_{gh}.

2.3. Energy of adsorption analysis

The potential energy of a molecule inside a host material, U_{gh}, is related to the heat of adsorption, Q_{st}, which is often considered as an indicator of the adsorbent heterogeneity since it is more sensitive to the microstructure than the adsorption isotherm itself.[23] The U_{gh} can be split into individual components, such as the drug–MOF chemical affinity and the adsorbate–adsorbate interactions, as a function of loading. In turn, both components of U_{gh} (adsorbate–adsorbent and adsorbate–adsorbate) influence the release process: the MOFs showing higher U_{gh} will provide longer release periods compared to MOFs with lower affinity.[23] Overall, the important variations in the adsorbate–adsorbent and adsorbate–adsorbate interactions give rise to different adsorption and release regimes.

Fig. 7 shows the U_{gh} results for the selected MOFs as a function of loading. Among those with available experimental data for drug entrapment and release kinetics, MIL-53 presents the highest U_{gh} at mid-high loadings (*ca.* -140 kJ mol^{-1}). It is interesting to note that the major contribution to U_{gh} is the adsorbate–adsorbent interactions, which remains almost constant throughout the adsorption process. In turn, the high, steady U_{gh} explains the experimentally observed long release process where the molecules are strongly retained by the framework (*i.e.* an almost constant release for up to 21 days).[3b] Even though our model of MIL-53 is rigid and does not take into account the framework flexibility, the obtained magnitude and the profile features of the U_{gh} are consistent with the observed delivery process. On the other hand, MIL-100 and MIL-101 present smaller U_{gh} values than MIL-53 at high loadings (*ca.* -130 and -85 kJ mol^{-1}, respectively), with an important contribution of the adsorbate–adsorbate component and a continued decrease of the adsorbate–adsorbent contribution when the loading increases. The impact of the adsorbate–adsorbent decrease in the total U_{gh} is particularly important in the case of MIL-100. The lower affinity for the IBU at mid-high loadings leads to shorter delivery times, as observed experimentally.

The U_{gh} of MIL-100 is larger than that of MIL-101 due to the narrower pores of MIL-100. Regarding the magnitude of U_{gh} at zero loading for MIL-100, simulations result in high values for both the full-access structure simulations and the pore-blocked one (*ca.* -150 kJ mol^{-1}), higher than MIL-53 due to the interaction with the coordinatively unsaturated Fe sites. However, this value could be overestimated when compared with the available drug-release experimental data, since the reported required time to discharge the IBU content from MIL-100 (*i.e.* 3 days) is half of that from MIL-101 (*i.e.* 6 days).[3a] This fact is highly striking, since the larger cavities of MIL-101 compared to MIL-100 and a similar surface chemistry and topology should imply weaker adsorbate–adsorbent interactions, higher diffusivity coefficients and therefore faster kinetics (see for example Haldoupis *et al.*[23]). Indeed, the existence of stronger interactions in MIL-100 compared to MIL-101 has been confirmed previously using experimental adsorption calorimetry by Llewellyn *et al.*[24] (for CH_4 and CO_2) and Trung *et al.*[25] (for C5–C9 *n*-alkanes).

The obtained profiles of U_{gh} *vs.* loading seem to show two regimes for both MIL-100 and MIL-101: the first one with relatively high U_{gh} values is related to the adsorption of the first

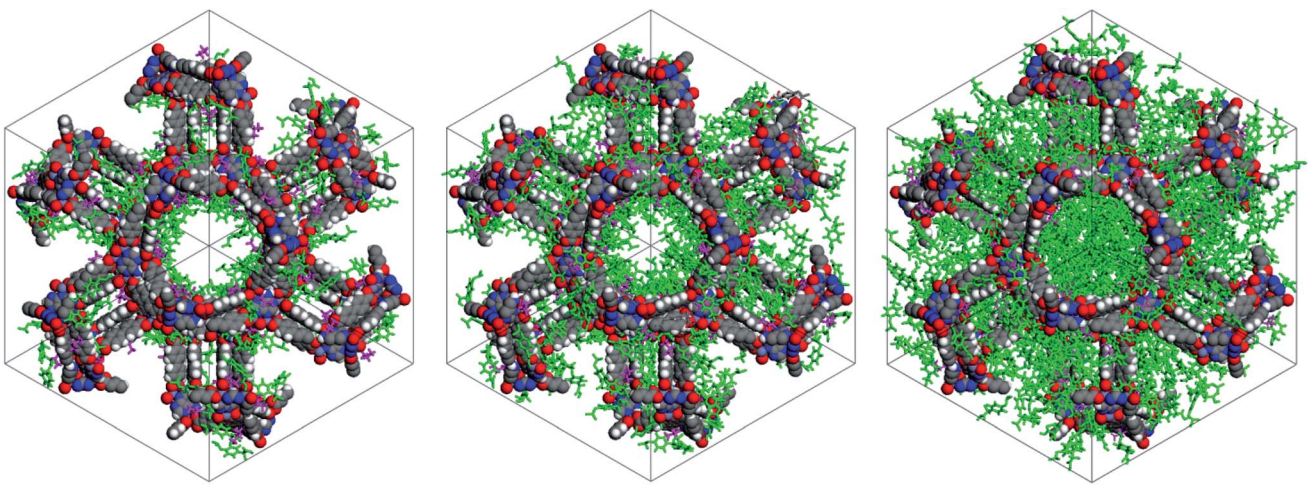

Fig. 6 Snapshots of ibuprofen in BioMOF-100 at different uptakes: 329 mg g^{-1} (left), 1095 mg g^{-1} (center) and 1975 mg g^{-1} (right). Ibuprofen molecules are shown in green stick-mode and DMA cations in pink stick-mode.

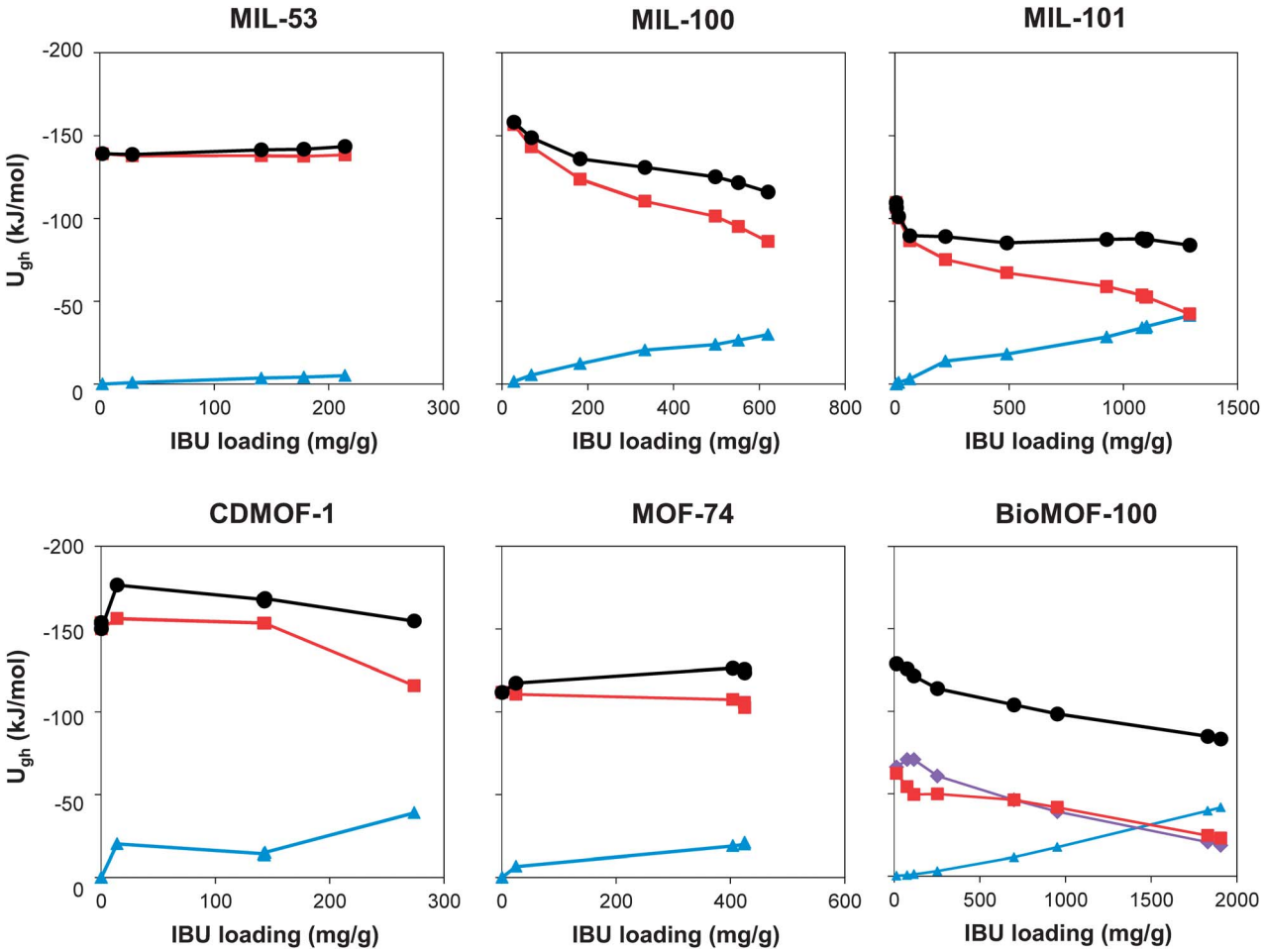

Fig. 7 Potential energy (U_{gh}) of IBU in a series of MOFs. The adsorbate–adsorbent component of U_{gh} is shown in red squares, the adsorbate–adsorbate component in blue triangles and the total U_{gh} in black circles. DMA–IBU interaction in BioMOF-100 is shown in purple diamonds. Note the existence of two and one steps in the adsorption isotherms of CDMOF-1 and MOF-74, respectively, and the existence of data points at very specific loadings.

molecules on the empty windows in both cavities simultaneously (except for blocked-MIL-100 simulations, where molecules first adsorb on the wider mesoporous cages). As the adsorption process continues, the adsorbate–adsorbent component gradually decreases, whereas the adsorbate–adsorbate component increases. The second regime, starting at *ca.* 500 and 1000 mg g^{-1} for MIL-100 and MIL-101, respectively, is associated with the adsorption of additional IBU molecules far away from the walls during the condensation at the center of the cavities. This leads to low adsorbate–adsorbent interactions and a marked increase of the adsorbate–adsorbate interactions.

According to these results, the first release regime on drug delivery experiments on MIL-100 and MIL-101 would involve the discharge of the molecules that are at the center of the cavities (*i.e.* the ones represented at higher loadings in Fig. 7) and therefore do not interact directly with pore walls. The second regime is due to the diffusion of those molecules that are strongly interacting with the adsorbent (*i.e.* the ones represented at lower loadings). In the case of MIL-101, according to the reported results,[3a] the differences in window sizes of small and large cavities seem to cause the split of the second regime into two independent regimes, an aspect that is not reflected in our simulations.

From the new proposed MOFs, CDMOF-1 presents the highest U_{gh} values at mid-high loadings (*ca.* 160 kJ mol^{-1}), followed by MOF-74 (*ca.* 125 kJ mol^{-1}) and BioMOF-100 (*ca.* 85 kJ mol^{-1}). CDMOF-1 and MOF-74 present channels with similar diameters to that of MIL-53. They also present U_{gh} profiles where the adsorbate–adsorbent component remains relatively constant with the loading (only small decreases on the adsorbate–adsorbent component are observed at high loadings), suggesting that the release process will also be controlled and gradual. The presence of polar groups and open metal sites in CDMOF-1 and MOF-74, respectively, results in higher values of U_{gh}, which at the end will be related to very long release times. In the case of BioMOF-100, having an outstanding pore volume and large mesopores, we would expect that the interactions between the adsorbent and the adsorbate were much lower than the previous cases, decreasing rapidly when the number of adsorbed IBU molecules increases. However, the IBU molecules also exhibit very important attractive interactions with DMA cations present in the pores. The adsorbate–

adsorbate component increases also linearly when increasing the loading. According to these results, BioMOF-100, which exhibits the highest IBU adsorption capacity among all the studied MOFs, would present a long controlled kinetic release comparable to the MIL-101 system.

Conclusions

We have used GCMC simulations to study the capacity and thermodynamic adsorption process of the model drug ibuprofen in state-of-the-art MOF materials. Our methodology allowed us to obtain a successful prediction of the drug adsorption properties of porous adsorbents. As a result, the comparison of the simulated capacities with the experimental reported values was highly consistent for MOFs with different pore geometries, such as uniform 1D microporous channels (*e.g.* MIL-53) and mesoporous spherical cavities accessible through wide windows (*e.g.* MIL-100, -101). In the case of MIL-100, simulations were close to experimental values when blocking the drug access to the narrower mesoporous cavities. Further differences might reflect the existence of experimental issues during the drug loading process or difficulties in complete sample activation. In addition, GCMC simulations allowed us to study new porous materials as potential drug carriers before running any experiments. In particular, the high energy of adsorption observed for CDMOF-1 suggests a potential controlled release process for this material. In the case of BioMOF-100, our simulations predict an outstanding IBU capacity of 1969 mg g^{-1}, six times higher than values found in mesoporous silicas. The presence of DMA cations in the pores that reinforce the attractive interactions with the IBU molecules will allow a slow kinetic release, comparable to the one found in MIL-101.

The description of the adsorption isotherm shapes, together with snapshots and RDF analysis, contributed to understand the adsorption process in the MOFs at a molecular level. The U_{gh} dependency on ibuprofen loading showed a good correlation with the experimental delivery process. By comparing the variation of U_{gh} in the proposed drug carriers MOF-74, CDMOF-1 and BioMOF-100 with the previously studied MIL-53, -100 and -101, we were able to infer about the most probable drug release process in these new materials. This work represents a complete GCMC simulation study that systematically analyses a set of MOF systems as potential drug carriers, proposing new tools for the corroboration of new, future experimental results.

Simulation methods

The adsorption of ibuprofen was investigated using grand canonical Monte Carlo (GCMC) simulations, performed with the multi-purpose code RASPA,[26] at 310 K (*i.e.* 37 °C). We used an atomistic model for all MOF structures, in which the framework atoms were kept fixed at their crystallographic positions. Ibuprofen–ibuprofen and ibuprofen–framework interactions were calculated using a Lennard-Jones (LJ) + Coulomb potential. LJ parameters for the framework atoms were taken from the Universal Force Field (UFF) (Fig. S7 and S8; Table S2, ESI†).[27] The ibuprofen molecule was constructed and modeled as flexible using TraPPE force fields (Fig. S8 and Table S3, ESI†).[28] Lorentz–Berthelot mixing rules were used for all cross-terms, and LJ interactions beyond 12 Å were neglected. Coulomb interactions were calculated using partial charges on the atoms, obtained by a charge equilibration method.[29] The Ewald sum method was used to compute the electrostatic interactions. Up to 10^6 Monte Carlo equilibration cycles and 10^6 production cycles were performed to calculate the ensemble averages. In one cycle, N moves were performed, where N is the number of molecules in the system (which fluctuates in GCMC). Monte Carlo moves used with equal probability were translation, rotation, insertion, deletion, random reinsertion, and regrowth of an existing molecule. In the case of BioMOF-100, simulations to compute the siting of dimethylammonium (DMA) cations present in the pores were performed previous to the simulations that included IBU (see ESI†).

The pore volume was obtained using a Widom particle insertion method, by probing the structure with a helium molecule at room temperature.[30] Accessible surface areas represented in the figures in the text were obtained using Materials Studio.[31] Ensemble averaged geometric details were obtained from radial distribution plots (RDF) from the GCMC simulations. The average potential energy of ibuprofen inside the host framework, $\langle U_{gh} \rangle$, was monitored. U_{gh} is related to the heat of adsorption, Q_{st}, as

$$-Q_{st} = \Delta H = \left(\frac{\partial \langle U_{gh} \rangle}{\partial \langle N \rangle} \right) - \langle U_g \rangle - RT$$

where N is the number of adsorbed molecules, U_g is the potential energy of the adsorbate in the ideal gas reference state, and R and T are the gas constant and temperature, respectively.[32] The adsorbate–adsorbent and adsorbate–adsorbate contributions of the average potential energy were calculated, as well.

Acknowledgements

M.C.B., M.P. and A.J.R-P acknowledge the Research Projects PIP 112-201101-0615 (CONICET) and PICT-2010-1466 (The National Agency of Scientific and Technological Promotion, Argentina). M.C.B. gratefully acknowledges the Consejo Nacional de Investigaciones Científicas y Técnicas (CONICET) for a Postdoctoral Fellowship. D.F.-J. acknowledges the Royal Society (UK) for a University Research Fellowship, and R.Q.S. acknowledges the Defense Threat Reduction Agency (HDTRA1-10-1-0023).

Notes and references

1 (*a*) M. Arruebo, *Wiley Interdiscip. Rev.: Nanomed. Nanobiotechnol.*, 2012, **4**, 16–30; (*b*) G. Paul, S. Steuernagel and H. Koller, *Chem. Commun.*, 2007, 5194–5196; (*c*) A. Bögershausen, S. J. Pas, A. J. Hill and H. Koller, *Chem. Mater.*, 2006, **18**, 664–672.

2 (*a*) D. Peer, J. M. Karp, S. Hong, O. C. Farokhzad, R. Margalit and R. Langer, *Nat. Nanotechnol.*, 2007, **2**, 751–760; (*b*) T. M. Allen and P. R. Cullis, *Science*, 2004, **303**(5665), 1818–1822.

3 (*a*) P. Horcajada, C. Serre, M. Vallet-Regi, M. Sebban, F. Taulelle and G. Férey, *Angew. Chem., Int. Ed.*, 2006, **45**, 5974–5978; (*b*) P. Horcajada, C. Serre, G. Maurin, N. A. Ramsahye, F. Balas, M. Vallet-Regi, M. Sebban, F. Taulelle and G. Férey, *J. Am. Chem. Soc.*, 2008, **130**, 6774–6780; (*c*) A. C. McKinlay, R. E. Morris, P. Horcajada, G. Férey, R. Gref, P. Couvreur and C. Serre, *Angew. Chem., Int. Ed.*, 2010, **49**, 6260–6266; (*d*) P. Horcajada, T. Chalati, C. Serre, B. Gillet, C. Sebrie, T. Baati, J. F. Eubank, D. Heurtaux, P. Clayette, C. Kreuz, J.-S. Chang, Y. K. Hwang, V. Marsaud, P.-N. Bories, L. Cynober, S. Gil, G. Férey, P. Couvreur and R. Gref, *Nat. Mater.*, 2010, **9**, 172–178; (*e*) J. Della Rocca, D. Liu and W. Lin, *Acc. Chem. Res.*, 2010, **44**(10), 957–968; (*f*) I. Imaz, M. Rubio-Martınez, L. Garcıa-Fernandez, F. Garcıa, D. Ruiz-Molina, J. Hernando, V. Puntesa and D. Maspoch, *Chem. Commun.*, 2010, **46**, 4737–4739; (*g*) J. An, S. J. Geib and N. L. Rosi, *J. Am. Chem. Soc.*, 2009, **131**, 8376–8377; (*h*) C.-Y. Sun, C. Qin, X. L. Wang, G. S. Yang, K. Z. Shao, Y. O. Lan, Z. M. Su, P. Huang, C. G. Wang and E. B. Wang, *Dalton Trans.*, 2012, **41**, 6906–6909.

4 O. K. Farha, A. O. Yazaydın, I. Eryazici, C. D. Malliakas, B. D. Hauser, M. G. Kanatzidis, S. T. Nguyen, R. Q. Snurr and J. T. Hupp, *Nat. Chem.*, 2010, **2**, 944–948.

5 J. An, O. K. Farha, J. T. Hupp, E. Pohl, J. I. Yeh and N. L. Rosi, *Nat. Commun.*, 2012, **3**(604), 1–6.

6 (*a*) A. C. McKinlay, B. Xiao, D. S. Wragg, P. S. Wheatley, I. L. Megson and R. E. Morris, *J. Am. Chem. Soc.*, 2008, **130**, 10440–10444; (*b*) B. Xiao, P. S. Wheatley, X. B. Zhao, A. J. Fletcher, S. Fox, A. G. Rossi, I. L. Megson, S. Bordiga, L. Regli, K. M. Thomas and R. E. Morris, *J. Am. Chem. Soc.*, 2007, **129**, 1203–1209; (*c*) N. J. Hinks, A. C. McKinlay, B. Xiao, P. S. Wheatley and R. E. Morris, *Microporous Mesoporous Mater.*, 2010, **129**, 330–334.

7 (*a*) W. J. Rieter, K. M. Pott, K. M. L. Taylor and W. Lin, *J. Am. Chem. Soc.*, 2008, **130**(35), 11584–11585; (*b*) K. M. L. Taylor, A. Jin and W. Lin, *Angew. Chem., Int. Ed.*, 2008, **47**, 7722; (*c*) K. M. L. Taylor, J. Della Rocca, Z. Xie, S. Tran and W. Lin, *J. Am. Chem. Soc.*, 2009, **131**, 14261–14263.

8 (*a*) C. D. Nunes, P. D. Vaz, A. C. Fernandes, P. Ferreira, C. C. Romao and M. J. Calhorda, *Eur. J. Pharm. Biopharm.*, 2007, **66**, 357–365; (*b*) L. Mohanambe and S. Vasudevan, *J. Phys. Chem. B*, 2005, **109**, 15651–15658.

9 D. G. Fatouros, D. Douroumis, V. Nikolakis, S. Ntais, A. M. Moschovi, V. Trivedi, B. Khima, M. Roldo, H. Nazar and P. A. Cox, *J. Mater. Chem.*, 2011, **21**, 7789–7794.

10 (*a*) T. Chalati, P. Horcajada, P. Couvreur, C. Serre, G. Maurin and R. Gref, *Nanomedicine*, 2011, **6**(10), 1683–1695.

11 C. Gaudin, D. Cunha, E. Ivanoff, P. Horcajada, G. Chevé, A. Yasri, O. Loget, C. Serre and G. Maurin, *Microporous Mesoporous Mater.*, 2012, **157**, 124–130.

12 R. Babarao and J. Jiang, *J. Phys. Chem. C*, 2009, **113**, 18287–18291.

13 (*a*) S. Bauer, C. Serre, T. Devic, P. Horcajada, J. Marrot, G. Férey and N. Stock, *Inorg. Chem.*, 2008, **47**, 7568–7576.

14 P. D. C. Dietzel, R. Blom and H. Fjellvag, *Eur. J. Inorg. Chem.*, 2008, **23**, 3624–3632.

15 (*a*) R. A. Smaldone, R. S. Forgan, H. Furukawa, J. J. Gassensmith, A. M. Z. Slawin, O. M. Yaghi and J. F. Stoddart, *Angew. Chem., Int. Ed.*, 2010, **49**, 8630–8634; (*b*) R. S. Forgan, R. A. Smaldone, J. J. Gassensmith, H. Furukawa, D. B. Cordes, Q. Li, C. E. Wilmer, Y. Y. Botros, R. Q. Snurr, A. M. Z. Slawin and J. F. Stoddart, *J. Am. Chem. Soc.*, 2012, **134**, 406–417.

16 L. D. Gelb and K. E. Gubbins, *Langmuir*, 1998, **15**, 305–308.

17 P. Horcajada, R. Greff, T. Baati, P. K. Allan, G. Maurin, P. Couvreur, G. Férey, R. E. Morris and C. Serre, *Chem. Soc. Rev.*, 2012, **112**, 1232–1268.

18 Q. He and J. Shi, *J. Mater. Chem.*, 2011, **21**, 5845–5855.

19 P. Horcajada, C. Márquez-Alvarez, A. Rámila, J. Pérez-Pariente and M. Vallet-Regi, *Solid State Sci.*, 2006, **8**(12), 1459–1465.

20 D. Fairen-Jimenez, Y. J. Colon, O. K. Farha, Y.-S. Bae, J. T. Hupp and R. Q. Snurr, *Chem. Commun.*, 2012, **48**, 10496–10498.

21 (*a*) D. Fairen-Jimenez, N. A. Seaton and T. Düren, *Langmuir*, 2010, **26**, 14694–14699; (*b*) J. Rouquerol, F. Rouquerol and K. S. W. Sing, *Adsorption by Powders and Porous Solids*, Academic Press, San Diego, CA, 1999.

22 T. Vuong and P. A. Monson, *Langmuir*, 1996, **12**, 5425–5432.

23 E. Haldoupis, S. Nair and D. S. Sholl, *Phys. Chem. Chem. Phys.*, 2011, **13**, 5053–5060.

24 P. L. Llewellyn, S. Bourrelly, C. Serre, A. Vimont, M. Daturi, L. Hamon, G. De Weireld, J.-S. Chang, D.-Y. Hong, Y. K. Hwang, S. H. Jhung and G. Férey, *Langmuir*, 2008, **24**(14), 7245–7250.

25 T. K. Trung, N. A. Ramsahye, P. Trens, N. Tanchoux, C. Serre, F. Fajula and G. Férey, *Microporous Mesoporous Mater.*, 2010, **134**(1–3), 134–140.

26 D. Dubbeldam, S. Calero, D. E. Ellis and R. Q. Snurr, *RASPA 1.0*, Northwestern University, Evanston, IL, 2008.

27 A. K. Rappé, C. J. Casewit, K. S. Colwell, W. A. Goddard III and W. M. Skiff, *J. Am. Chem. Soc.*, 1992, **114**, 10024–10035.

28 (*a*) N. Rai and J. I. Siepmann, *J. Phys. Chem. B*, 2007, **111**, 10790–10799; (*b*) S. Clifford, K. Bolton and D. Ramjugernath, *J. Phys. Chem. B*, 2006, **110**, 21938–21943; (*c*) J. M. Stubbs, J. J. Potoff and J. I. Siepmann, *J. Phys. Chem. B*, 2004, **108**, 17596–17605; (*d*) C. D. Wick, M. G. Martin and J. I. Siepmann, *J. Phys. Chem. B*, 2000, **104**, 8008–8016; (*e*) M. G. Martin and J. I. Siepmann, *J. Phys. Chem. B*, 1999, **103**, 4508–4517; (*f*) C. D. Wick, J. M. Stubbs, N. Rai and J. I. Siepmann, *J. Phys. Chem. B*, 2005, **109**, 18974–18982.

29 C. E. Wilmer, K. C. Kim and R. Q. Snurr, *J. Phys. Chem. Lett.*, 2012, **3**, 2506–2511.

30 (*a*) A. Leach, *Molecular modelling: principles and applications*, Pearson Prentice Hall, 2001; (*b*) A. L. Myers and P. A. Monson, *Langmuir*, 2002, **18**, 10261–10273.

31 *Materials Studio v6.1*. Accelrys Software Inc., San Diego, CA 92121, USA.

32 D. Nicholson and N. G. Parsonage, *Computer Simulation and the Statistical Mechanics of Adsorption*, Academic Press, London1982.

